Supporting Information

Flexible CoFeB/silk Films for Biocompatible RF/microwave Applications

Qi Zhang[†], Bin Peng[‡], Yanan Zhao[‡], Chunlei Li[‡], Shukai Zhu[‡], Keqing Shi[§], Ziyao Zhou[‡], Xiaohui Zhang[†], Ming Liu[‡]*, Jingye Pan[§]**

[†] The Key Laboratory of Biomedical Information Engineering of Ministry of Education, School of Life Science and Technology, Xi'an Jiaotong University, Xi'an 710049, PR China

[‡] Electronic Materials Research Laboratory, Key Laboratory of the Ministry of Education & State Key Laboratory for Mechanical Behavior of Materials, Xi'an Jiaotong University, Xi'an, Shaanxi 710049, China

[§] Department of Intensive Care, Precision Medicine Center Laboratory, The First Affiliated Hospital of Wenzhou Medical University, Wenzhou 325000, PR China

*Corresponding Author: Xiaohui Zhang (E-mail: xiaohuizhang@mail.xjtu.edu.cn); Ming Liu (E-mail: mingliu@xjtu.edu.cn); Jingye Pan (panjingye@wzhospital.cn).

1. Characterization of surface morphology and mechanical properties

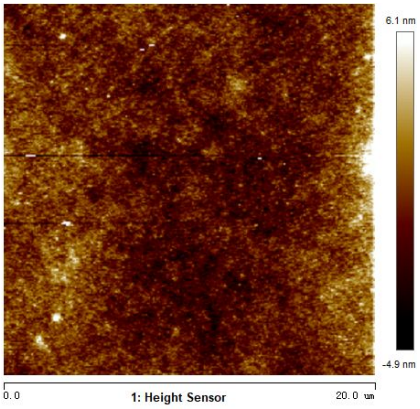

Figure S1. AFM image of the silk film substrate. The roughness value of the displayed area is Ra = 1.1 nm.

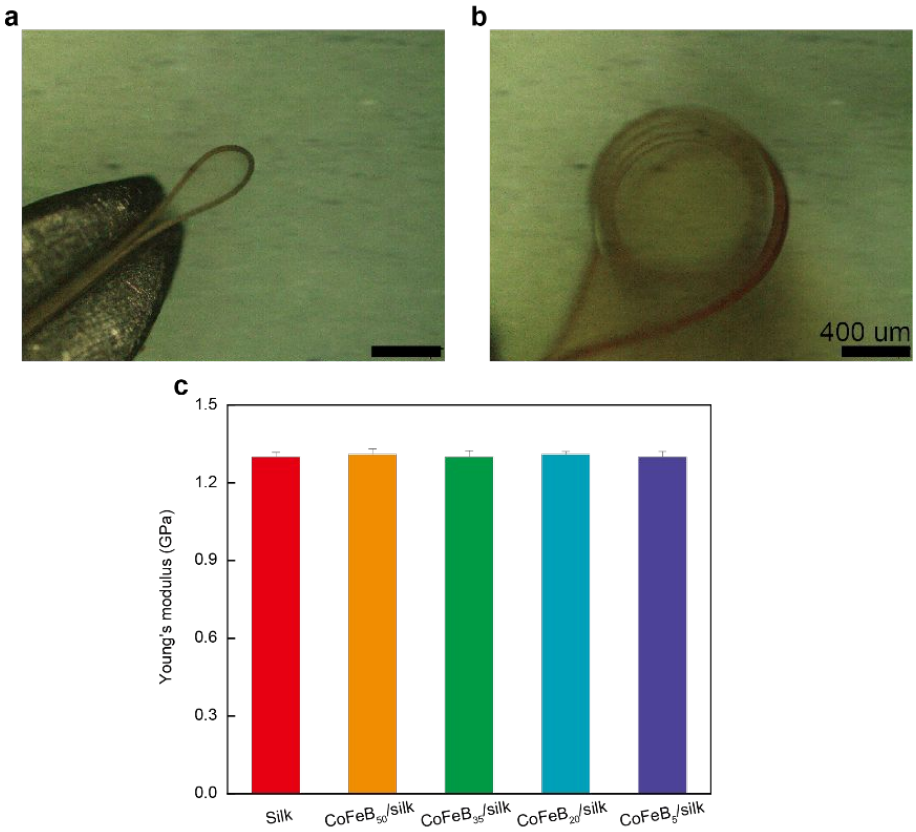

Figure S2. Mechanical properties of CoFeB/silk films. Bending (a) and curl (b) of the CoFeB/silk film; (c) Young's modulus of CoFeB/silk films with different thickness of CoFeB layer.

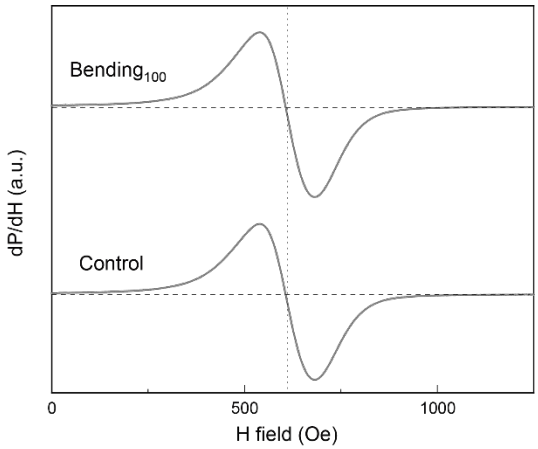

Figure S3. In-plane FMR field of CoFeB/silk films after 100 cycles of bending.

2. The biocompatibility of CoFeB/silk films

To evaluate the biocompatibility of the CoFeB/silk film, we isolated and cultured adult skin fibroblasts on the films. The treated CoFeB/silk films were used in the biocompatibility study. As shown in Figure S4, the cells cultured on the CoFeB/silk films exhibited >99% cell viability, which has no significant difference from the control group. These results indicate the excellent biocompatibility of the CoFeB/silk films.

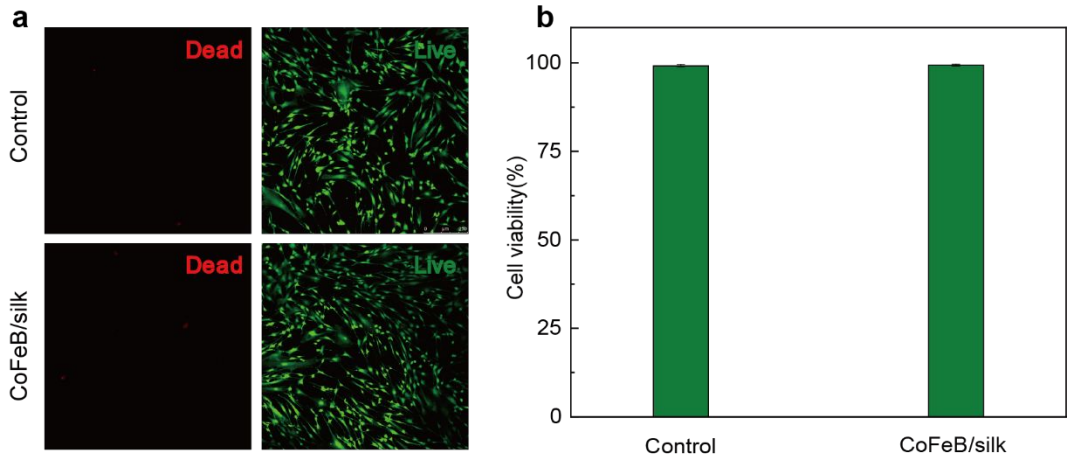

Figure S4. Live/Dead staining of skin fibroblasts cultured on the CoFeB/silk films and TCPs for 48 hours. (a) live-dead staining of skin fibroblasts. (b) viability of skin fibroblasts.

3. ESR tests of 35-nm CoFeB/silk films along the in-plane direction

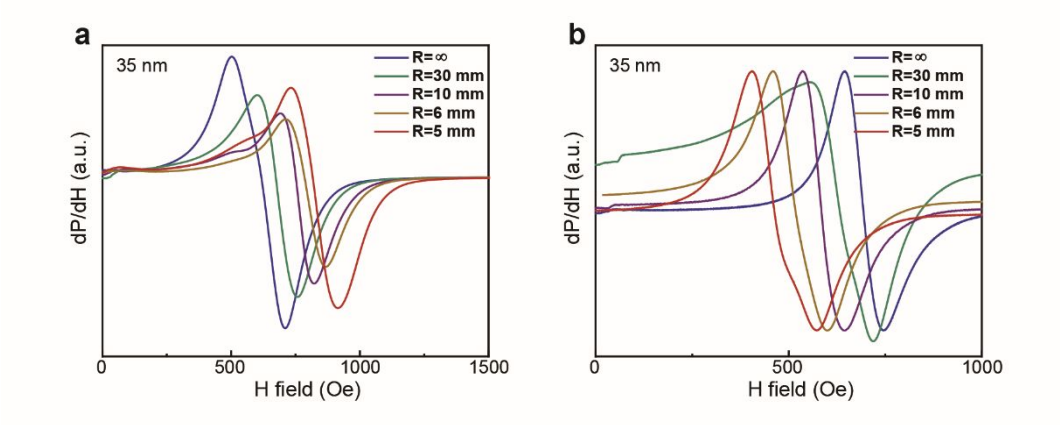

Figure S5. Ferromagnetic field of 35-nm CoFeB/silk films with different bent radius along the in-plane direction. (a) compression; (b) tension.

4. The controllable dissolvability of CoFeB/silk films

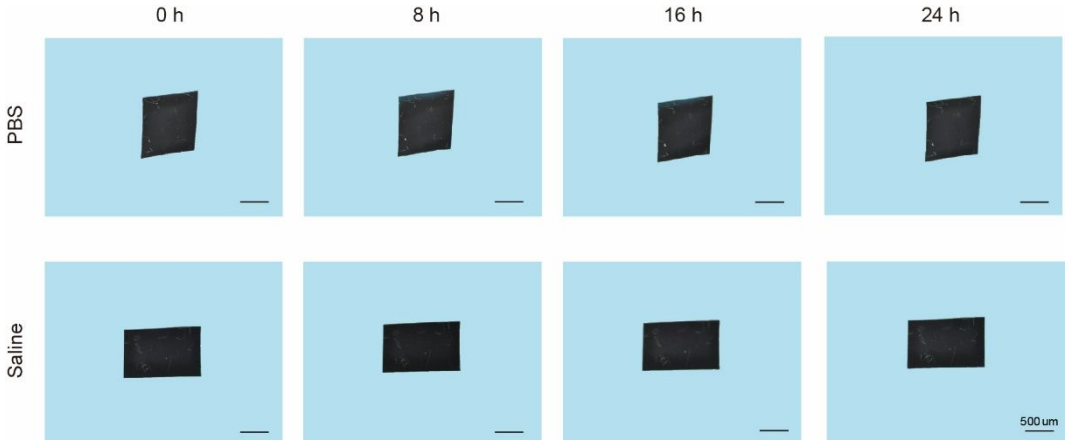

Figure S6. Images of the treated CoFeB/silk films post-immersion in PBS and saline for 0, 8, 16, and 24 hours, respectively.

5. In-plane FMR spectra of 20-nm CoFeB/silk films

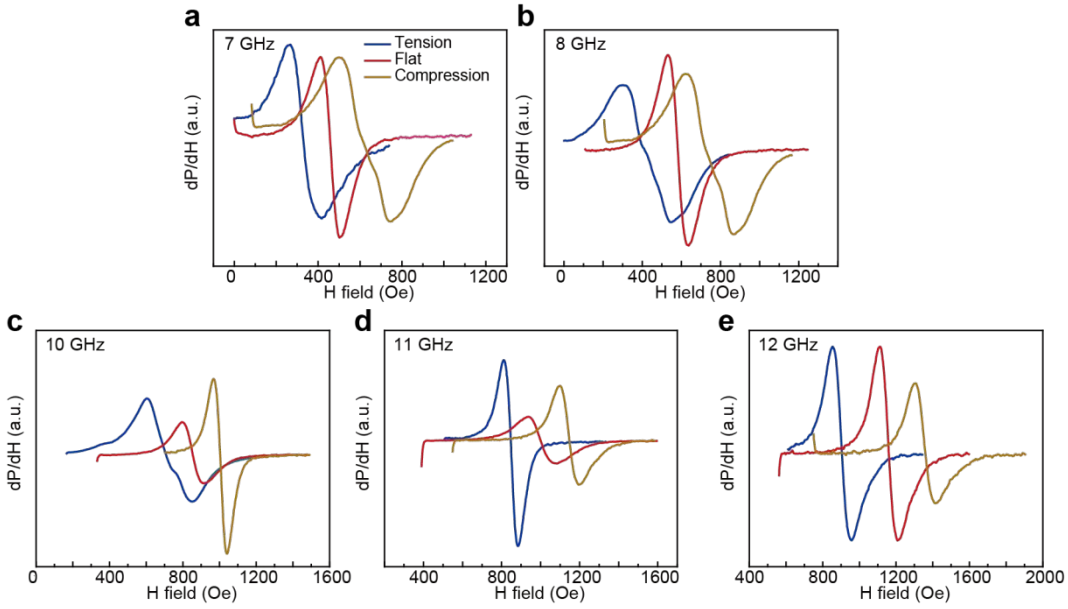

Figure S7. The tunable in-plane FMR Hr spectra at 7 GHz (a), 8 GHz (b), 10 GHz (c), 11 GHz (d) and 12 GHz (e).

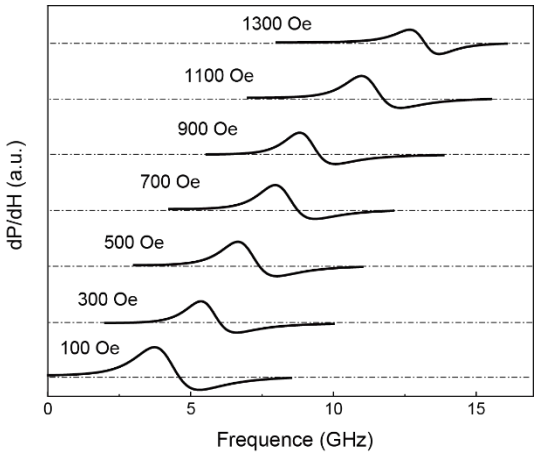

Figure S8. The FMR frequency spectra under different external magnetic bias fields.

6. The magnetic hysteresis (M-H) loops of the CoFeB/silk films

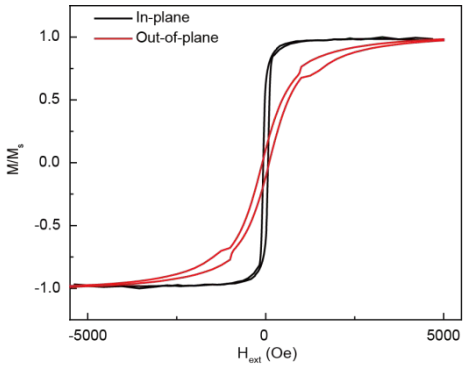

Figure S9. M-H loops under the flat state along the in-plane (blue line) and out-of-plane direction (red line).

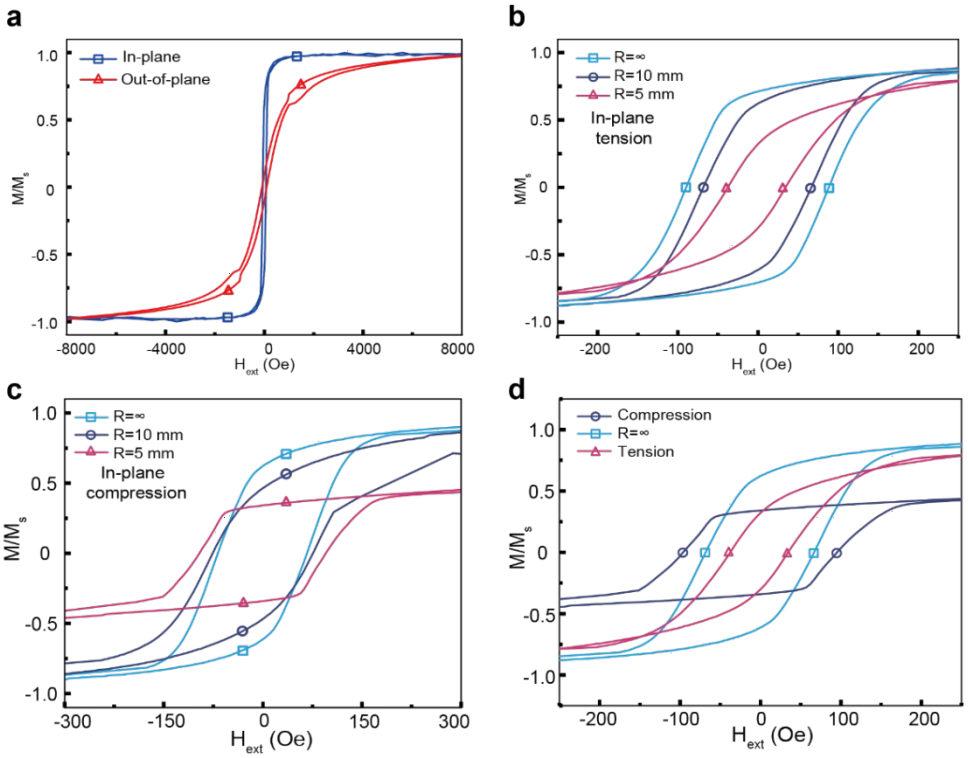

Figure S10. (a) M-H loops under a flat state along the in-plane and out-of-plane direction. M-H loops under tensile stress (b) and compressive stress (c) along the in-plane direction with different bending radii (20-nm CoFeB films). (d) M-H loops under tensile and compressive stress along the in-plane direction (20-nm CoFeB films).

7. Stability in air of CoFeB/silk films

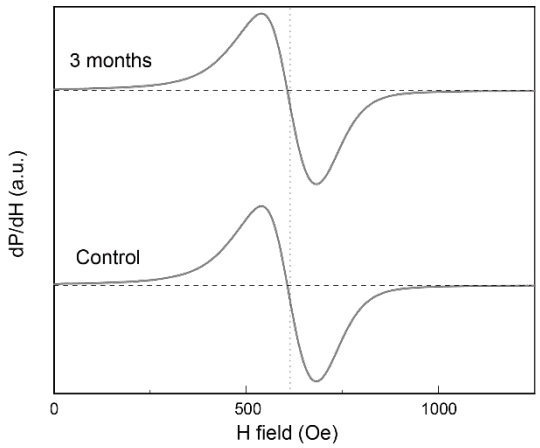

Figure S11. In-plane FMR spectrum of CoFeB/silk films freshly prepared and after three months of exposure in air.

8. Wireless strain sensing for motion monitoring based on the flexible CoFeB/silk film

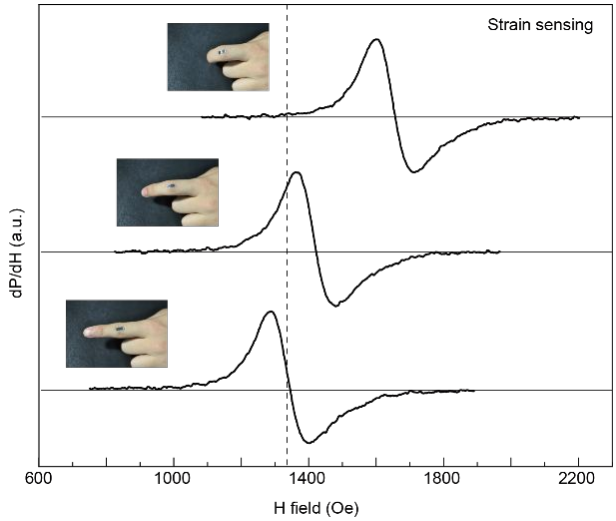

Figure S12. Offset of FMR spectra during finger joint bending.

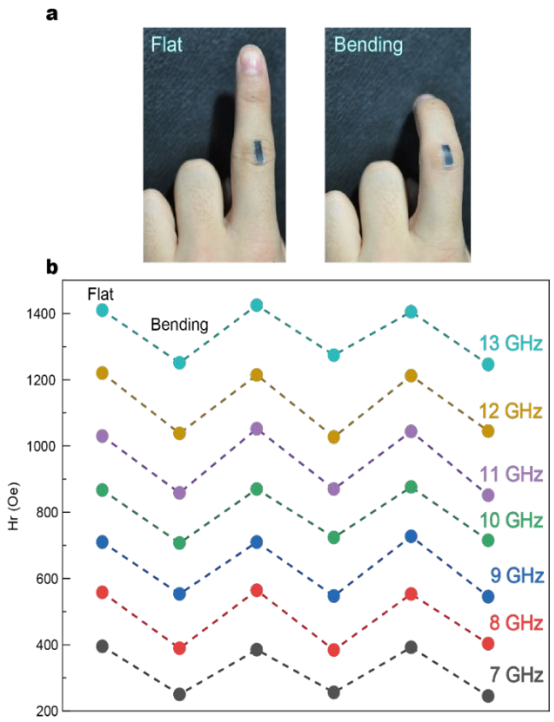

Figure S13. Wireless sensing of finger joint motion: (a) Photographs of the CoFeB/silk film affixed to the finger joint. (b) Sensing at multiple operating frequencies.